WPPMI-PR(17) 18499

MD Kovari et al.

A one-dimensional scrape-off layer model in the reactor systems code PROCESS

Preprint of Paper to be submitted for publication in
Fusion Engineering and Design

This work has been carried out within the framework of the EUROfusion Consortium and has received funding from the Euratom research and training programme 2014-2018 under grant agreement No 633053. The views and opinions expressed herein do not necessarily reflect those of the European Commission.

A one-dimensional scrape-off layer model in the reactor systems code 'PROCESS'

M Kovari * [1], A. Kallenbach[2], M. Siccinio[2, 3]

[1] EURATOM/CCFE Fusion Association, Culham Science Centre, Abingdon, Oxon, OX14 3DB, UK
[2]Max-Planck Institute for Plasma Physics, Garching, Germany
[3] EUROfusion Consortium, Garching, Germany
*Corresponding author. Tel.: +44 (0)1235-46-6427. E-mail address: michael.kovari@ukaea.uk

Abstract

We have implemented a one-dimensional scrape-off layer (SOL) model in the PROCESS fusion reactor systems code. It allows reactor scenarios to be obtained while limiting both the plasma temperature of the SOL at the entrance to the sheath at the divertor target, and the power density on the target. To take account of cross-field transport in an *ad hoc* way, the area of the flux tube is increased discontinuously part of the way along its length. The following physical processes are included: convected heat flux; thermal conduction; momentum conservation; radiation by deuterium, tritium and impurities; charge exchange; electron impact ionisation; and surface recombination. Pumping is not included – all particles striking the target are recycled. The strong shearing of the flux tube near the X-point is not taken into account. The isotropic emission of fast neutrals due to charge exchange from the part of the SOL adjacent to the target dominates the total power density on the target when the plasma temperature is reduced below 5 eV.

As the seeded impurity concentration is increased a discontinuous transition is observed between an attached state where the plasma temperature at the target is 50 eV, and a state where the temperature at the target hits the lower bound of the simulation, 1.1 eV. We interpret this as a detached state, within the limitations of the model.

Keywords: tokamak, scrape-off layer, detachment

1. Introduction

A reactor systems code includes simple models of all parts of a reactor system, from the basic plasma physics to the generation and transmission of electricity. We have implemented a modified version of a one-dimensional scrape-off layer (SOL) model developed by Kallenbach et al [1] in the PROCESS [2] fusion reactor systems code. Only the outer divertor is included, as there are reasons to believe that a 1D approach is not suitable for the inner divertor leg [1]. The typical connection length from the outboard side of the plasma to the inner target is about three times as long as that to the outer target, giving time for extensive broadening of the SOL. The outer target receives the majority of the divertor heat load, concentrated in a narrower profile than at the inner target [3]. Experience with single-null divertors shows that if the power density on the outer target is acceptable then so is the power on the inner target [4]. If the outer divertor has an X or Super-X configuration, it may detach while the inner divertor is still attached, but these configurations are not considered here. The model allows optimised reactor scenarios to be obtained while limiting both the plasma temperature of the SOL at the entrance to the sheath at the divertor target, and the power density on the target.

A recent study using the SOLPS code [5] proposed argon as a seeded impurity, the electron temperature adjacent to the target < 5 eV and the peak heat flux < 5 - 10 MW/m^2. However, when the radiation on the target was taken into account, the peak heat flux on the outer target could not be reduced below 15 MW/m^2. This underlines the importance of optimising the main plasma and SOL as a single system. A study using the SONIC code found that a self-consistent scenario could be found using argon seeding only, achieving full detachment at the inner target and partial detachment at the outer target [6].

2. The SOL model

We have used equations 2-7 from [1], but rewritten as a set of ordinary differential equations in the six dependent variables listed in Table 1. The other quantities such as ν are calculated from these. The independent variable x is the distance along the field line from the divertor target. Parameter names used more than once are given in Table 2. Throughout this paper, quantities referred to as "at the target" should be understood to be defined at the entrance to the target sheath.

The neutral deuterium and tritium flux from the target is divided into two velocity groups each carrying half the flux. The first group of atoms has a bulk velocity of ¼ of the mean thermal speed corresponding to a temperature of 5 eV, representing the typical kinetic energy of atoms after electron impact dissociation (Franck–Condon atoms [7])

and reflection of sheath-accelerated ions. The second group is started at the target with a nominal bulk velocity higher by a factor 10. This choice was guided by the small angle pitch angle of the field line, which allows neutrals entering from the side to enter the flux tube at a relatively large connection length from the target. These velocities are assigned just to calculate a penetration depth – when the neutrals become part of the plasma by ionisation, their energy and momentum are set to zero. The ionization rate is also calculated assuming the neutrals are at rest. We have found that the value of the velocity multiplier does not have a big effect on the results. The effect of impurity ions on radiation and on thermal conductivity has been taken into account, but their contribution to electron density is neglected.

Table 1. Dependent variables

n_{01}	Number density of group 1 (slow) neutral atoms.
n_{02}	Number density of group 2 (fast) neutral atoms.
(nv)	$n = n_e = n_i$ (electron and ion density), and v is the plasma flow velocity
T	$T = T_e = T_i$ is the plasma temperature
P_{tot}	$\left(m_i v^2 + 2eT\right)$
Q	Power transported along the SOL

Table 2. Derived parameters.

c_{s0}	Ion sound speed at the target
A_0	Area of SOL at the target
R_{ion}	Rate coefficient for ionisation of hydrogenic species by electron impact
R_{rec}	Rate coefficient for volume recombination of hydrogenic species
R_{CX}	Rate coefficient for charge exchange of hydrogenic species

There are four additional differential equations to calculate the integrals of the power loss terms. The sum of these losses is used to check the power balance. As the pressure P_{tot} has been used as an independent variable, we need to solve the quadratic equation of P_{tot} to give the plasma density. (The correct solution can be identified by observing that at the midplane the bulk velocity is zero, but the total pressure is non-zero.)

$$n = \frac{P_{tot} + \sqrt{P_{tot}^2 - 4 \cdot 2e\, m_i T_e (nv)^2}}{2 \cdot 2e\, T_e} \tag{1}$$

The equations used are as follows. (Heat flux and velocity towards the target are negative.)

Continuity equation for “slow” neutrals:

$$\frac{d n_{01}}{dx} = \frac{1}{v_{01}} \left(R_{rec} n^2 - R_{ion} n_{01} n \right) \tag{2}$$

Continuity equation for “fast” neutrals:

$$\frac{d n_{02}}{dx} = \frac{-1}{v_{02}} R_{ion} n_{02} n \tag{3}$$

Convected heat flux:

$$q_{\parallel conv} = -(nv)\left(5eT + \frac{1}{2}m_i\left(\frac{nv}{n_e}\right)^2\right) \tag{3}$$

The cross-section area of the SOL, A, is calculated by taking the radial width equal to the power fall-off length. Total heat flux is derived from the total power in the SOL, *Q*:

$$q_{\parallel total} = \frac{Q}{A} \tag{4}$$

Total heat flux is the sum of the convected and conducted fractions, therefore the conducted fraction is:

$$q_{\parallel cond} = q_{\parallel total} - q_{\parallel conv} \tag{5}$$

For thermal conductivity there is no general expression for a multi-species plasma, but an approximation has been proposed by [8]:

$$\kappa_0 \approx \frac{8788}{Z_{eff}}\left(\frac{Z_{eff} + 0.21}{Z_{eff} + 4.2}\right)\frac{W}{m \cdot e V^{7/2}}, \tag{6}$$

where Z_{eff} is the effective ion charge (taken as constant throughout the SOL), and ion conductivity is neglected. Thermal conduction is then described by

$$\frac{dT}{dx} = q_{\parallel cond}\frac{1}{T^{2.5}\kappa_0} \tag{7}$$

Ion continuity:

$$\frac{d(nv)}{dx} = R_{ion}n_{01}n + R_{ion}n_{02}n - R_{rec}n^2 \tag{8}$$

Momentum conservation:

$$\frac{dP_{tot}}{dx} = -\left(R_{CX}(n_{01} + n_{02}) + R_{rec}n\right)(nv)m_i \tag{9}$$

Impurity radiation loss density:

$$\rho_{imp} = n^2\sum_Z c_Z L_Z \tag{10}$$

L_z = radiative loss function for impurity species $z\left(W m^3\right)$

Radiation loss density for neutral hydrogenic species:

$$\rho_H = (n_{01} + n_{02})n(p_{ℓ} + p_{RB}) \tag{11}$$

$p_{ℓ}$ = line radiation power rate coefficient $\left(W m^3\right)$ p_{RB} = continuum radiation power rate coefficient $\left(W m^3\right)$

Charge exchange power loss density:

$$\rho_{CX} = e\, T_e\, R_{CX} \left(n_{01} + n_{02} \right) n \tag{12}$$

Ionisation power loss density:

$$\rho_{ion} = \left(R_{ion}\, n_{01} + R_{ion}\, n_{02} \right) e\, E_{ion} \tag{13}$$

Energy conservation:

$$\frac{dQ}{dx} = A \left(\rho_{imp} + \rho_H + \rho_{CX} + \rho_{ion} \right) \tag{14}$$

The PROCESS implementation allows thirteen impurities: He, Be, C, N, O, Ne, Si, Ar, Fe, Kr, Ni, W, Xe. The impurities other than helium are likely to be enriched in the SOL relative to the main plasma. Based on neoclassical transport it is predicted that for ITER there will be a net outward drift of tungsten in the pedestal provided the temperature is greater than 92 eV [9]. We expect the same to be qualitatively true for DEMO, and for other impurities with high atomic numbers such as argon.

Using ADAS data the ratios of different ionisation states for each impurity were calculated for a range of temperatures and a single electron density, 1×10^{20} m^{-3}. Radiative loss functions, mean ionic charge and mean squared ionic charge were calculated and tabulated as a function of the dwell time parameter describing the departure from local ionisation equilibrium in the SOL. For hydrogenic species, cross-section and rate tables are used for recombination, ionisation, charge exchange, line radiation and continuum radiation. For power balance the energies in Table 3 are used.

Table 3. Energies required for loss calculations

Volume recombination energy (assumed to be lost as radiation)	13.6 eV
Molecular association (per ion)	2.3 eV
$E_{rec} = ¿$ Surface recombination (including association)	15.9eV
$E_{ion} = ¿$ Electron energy loss due to ionization	15 eV

The effective charge is derived by summing contributions over all impurity elements *j*,

$$Z_{eff} = 1 + \sum_{j \neq H} c_j \left(\acute{Z}_j^2 - \acute{Z}_j \right) \tag{15}$$

where $\acute{Z}_j$ and $\acute{Z}_j^2$ are the mean charge and mean square charge averaged over the different ionisation states for impurity element j.

The connection length from midplane to target has been calculated by direct integration for an example reactor equilibrium (Figure 1). A fit to this curve has been used, as a function of Δr, the radial distance from the LCFS at the outer midplane. The connection length is taken to be proportional to $\pi R_0 q_{95}$, so the final estimate, with metre units, is

$$L_{con} = \frac{\pi R_0 q_{95}}{93.2} \left(21.25 \ln \left(\frac{1}{\Delta r} \right) - 8.7 \right) \tag{16}$$

The relevant distance Δr has been taken to be λ_{qOMP}, the power fall-off length in the SOL at the outer midplane. The large connection length and elongation of the flux tube cross-section very near the separatrix may be important, leading to strong cross-field transport, but this is not taken into account.

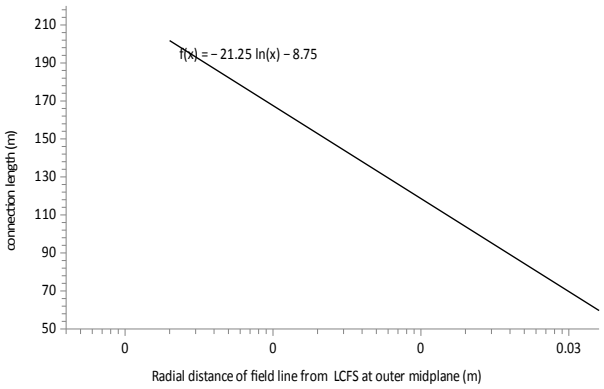

Figure 1. Connection length from outer midplane to divertor. Plasma major radius = 9.0734 m, toroidal field at axis = 5.6212 T, Safety factor at 95% flux surface = 3.2691, divertor is at major radius = 8.3 m.

The ordinary differential equations are solved using a modified divided difference form of the Adams PECE formulas [10]. At the point in the SOL when the neutral density becomes small (less than 10^{14} m^{-3}), all the atomic rates are set to zero and remain at zero for the remainder of the integration. This is essential to stop the equations being too stiff.

The total field is assumed to be constant along the flux tube. In the absence of cross-field transport the area of the flux tube would then be constant. To take account of cross-field transport in an *ad hoc* way, the width of the flux tube is increased discontinuously by a specified amount at a point given by a specified fraction of the total connection length.

The momentum factor, the ratio of momentum of the SOL plasma at the target to that at the midplane, is

$$f_{mom} = \frac{2 T_{target} n_{target}}{T_{midplane} n_{midplane}} \tag{17}$$

The sonic boundary condition at the target makes the factor of 2 appropriate.

3. Target physics and boundary conditions

The SOL strikes the target at an oblique angle, so a Chodura sheath is formed [11], except in detached conditions. The velocity of the ions along B at the entrance to the sheath is greater than or equal to c_s. The thickness of the sheath is

$$L_{Chodura} = \sqrt{6} \frac{kT}{e\, c_s B} \sin\psi\,, \tag{18}$$

where ψ is the angle between B and the surface normal (nearly 90º). The thickness is small compared to the divertor dimensions, at around 0.2 mm when the target temperature is 100 eV. To a good approximation the sink action of the solid surface acting on the plasma, with regard to both particle and power flows, is unaffected by the change from a normal to an oblique target, and the ion impact energy is also unaffected.

The ratio of the wetted area on the target to the area measured perpendicular to the field line is

$$f_s = \frac{1}{\cos\psi} = \frac{1}{\sin(\alpha)\dfrac{B_\theta}{B_{total}}} \tag{19}$$

where B_θ is the poloidal field, B_{total} is the total field, and α is the angle in the poloidal plane between the target and the projection of the field line onto the poloidal plane (Figure 2).

The plasma reaching the sheath is assumed to be sonic (Mach number = 1). The plasma flux at the target measured normal to the field is therefore

$$\Gamma = n_e c_{s0} \tag{20}$$

where n_e is the plasma density near the target. The heat flux due to convection and conduction, measured normal to the field, is

$$q_{\parallel} = \gamma e T_0 \Gamma \tag{21}$$

where γ is the sheath energy transmission coefficient, and $T_0$is the temperature at the target.

Here we want to start with the engineering parameters, so we obtain the electron density at the target, n_e, from q_{dep} , the power density on the target due to convection and conduction:

$$n_e = \frac{q_{dep} f_s}{\gamma e T_0 c_{s0}} \tag{22}$$

where $T_0$is the temperature at the target, and γ is the sheath energy transmission coefficient [11]. In estimating γ we ignore (i) the electrical bias of the target, (ii) secondary electron emission and electron reflection, and (iii) atom–atom recombination. The electron and ion contributions to γ, taking account of the reflection coefficient for ion energy, R_E, are

$$\gamma = \gamma_e + \gamma_{i,} \gamma_e = 5.5, \gamma_i = 2.5\left(1 - R_E\right). \tag{23}$$

According to the Chodura theory the ions strike the surface at right angles, but surface roughness implies that one should probably use values averaged over a range of angles of incidence. The fraction of the total kinetic energy that is reflected, R_E, is of the order of 50% for deuterium atoms in the range 1 – 100 eV striking a tungsten target [12]. We use the same figure for ions, assuming that the electron in an incident atom is absorbed into the conduction band of the target on a timescale shorter than the reflection process. The presence of tungsten "fuzz" due to prolonged ion bombardment would tend to trap incident particles, but we have neglected this effect on energy reflection. Electron-ion recombination of hydrogenic ions on the target is taken into account (but not included in γ) by adding the power

$$E_{rec} e n_e c_{s0} A_0 \tag{24}$$

where A_0 is the cross-section of the SOL at the target.

4. What happens to the lost energy?

The SOL emits energy by radiation and by charge exchange. (The energy lost by ionisation of neutrals is not considered to be emitted to the surroundings.) Although this energy is emitted isotropically, a substantial fraction nevertheless lands on the target. We have made a rough estimate of this fraction as follows. Figure 2 shows the target and SOL in the poloidal plane. The area on which this energy is mainly incident is shown by the red line, given by

$$A_{receiving} = 2 \cdot \text{Wetted Area} = 2\pi R_{target} \cdot 2W \tag{25}$$

where R_{target} is the major radius of the target and W is the wetted length of the target, measured in the poloidal plane (derived from the power fall-off length). The power emitted by the "near zone" is calculated by direct integration, and half is assumed to reach the target. (The power due to charge exchange atoms is reduced by the energy reflection coefficient.) The volume of the "near zone" of the flux tube depends on the connection length between A and B, s_{AB},

$$s_{AB} = L_{AB} \frac{\sqrt{B_p^2 + B_t^2}}{B_p} \tag{26}$$

where B_p is the local poloidal field and B_t is the local toroidal field, and the length AB in the poloidal plane is

$$L_{AB} = \frac{2W}{\cos\alpha} \tag{27}$$

where α is the angle of incidence in the poloidal plane.

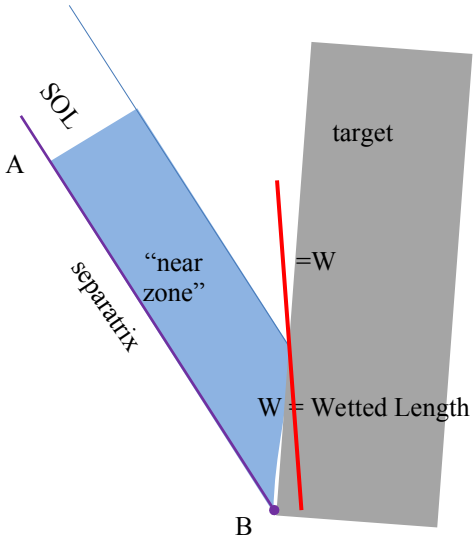

Figure 2. Target and SOL in the poloidal plane. The blue shaded area is considered "near" to the target, and energy loss from this area is used to calculate the extra load on the area of target shown by the red line.

This estimate is based on the assumption that the length of the radiative zone in the SOL (in the poloidal plane) is greater than the wetted length. Significant radiation is emitted from outside the "near zone", but does not add much to the local power deposition. If the radiative zone is of the order of the wetted length or less the formula above underestimates the power density landing on the wetted area. However, in reality neutrals will impinge on the SOL all along its length, not just from the direction of the target as assumed, so the radiative zone is likely to be larger than that calculated here.

5. Behaviour close to the target

This model does not give results within the sheath itself, but the zone immediately upstream of the sheath can still have surprisingly rapid gradients. Figure 3 shows the parameters in the SOL as a function of the distance from the divertor target, for target temperature = 10 eV. The 2 mm zone adjacent to the sheath entrance is shown in detail on the left side of the figure. The right hand side shows the remainder of the SOL on a log scale. The Mach number curve shows that much of the acceleration of the plasma approaching the target occurs in the last 0.2 mm, while the plasma density drops at the same time because of particle conservation. This suggests that finite Larmor radius effects and local variations in the shape of the target may be important. (Ion Larmor radius is ~0.14 mm.) Ionisation of the neutrals emerging from the target is largely complete over the first two millimetres.

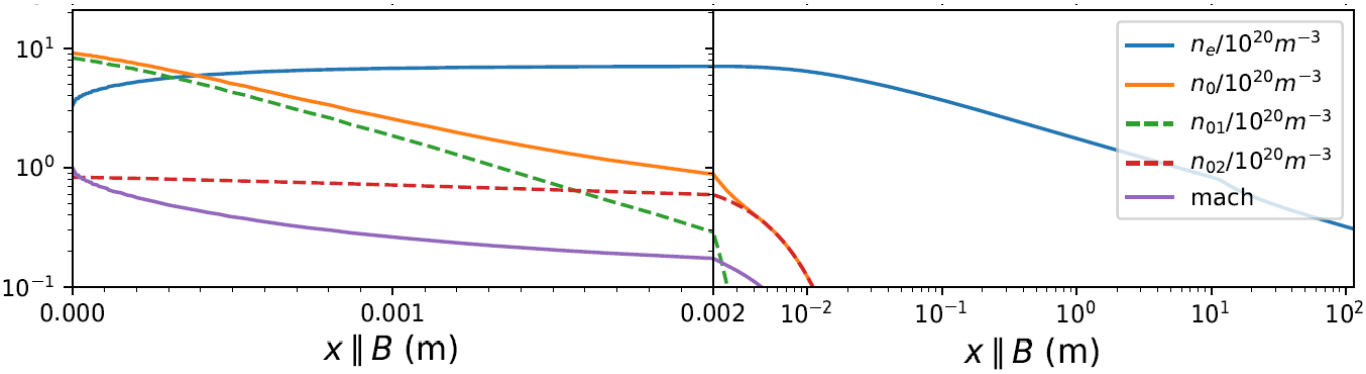

Figure 3. Parameters in the SOL as a function of the distance *x* from the divertor target. Target temperature = 10 eV. Other parameters as in Table 4 and Table 5.

Table 4. Selected input parameters used except where stated

Conversion from flux density [el/s] to Pascal [Molecules]	1.55×10^{23}
Ratio: Total power through separatrix / power at midplane directed towards outer target	2.3
Parameter for approach to local equilibrium	0.5×10^{17} s m^{-3}
SOL power fall-off length at the outer midplane	2 mm
SOL power fall-off length at the target	5 mm
Distance from target at which SOL gets broader as a fraction of connection length	0.1
Mean SOL density at OMP / separatrix density	0.9
Angle between flux surface and divertor target (α)	30º
Impurity enrichment (ratio of concentration in SOL to confined plasma):	
Helium	0.4
Other impurities [13]	5

6. Consequences for optimised reactor scenarios

The benefit of implementing the SOL model in the reactor systems code “PROCESS” is that many parameters can be varied simultaneously to optimise the selected figure of merit while satisfying the constraints. All the results in this paper have been obtained in this way. Some of the input parameters are shown in Table 4 and Table 5 (except where stated).

Figure 4 shows the plasma and neutral profiles in the SOL for a PROCESS solution where the target temperature is set to 1 eV. The first plot shows that with these inputs the SOL loses most of its momentum and energy in the last few millimetres before the target. This shows that that the decline of temperature along the SOL (plot two) is not an indication of loss of energy, but only of the increased density (plot three), described as plasma compression. In contrast to Figure 3, ionisation of the neutrals emerging from the target takes about 10 mm, because the temperature is too low at the target to cause ionisation. The high thermal conductivity in the upstream half of the SOL (note the log scale) enables the plasma to remain nearly isothermal in that region (eq. 7), but the stipulation of a low temperature at the target requires an increasing temperature gradient downstream. The lack of neutrals and low recombination rates in most of the SOL cause the pressure to be constant there (eq. 9). As plasma is not conserved, the speed and flux of the plasma can tend to zero towards the midplane. This model does not impose any boundary condition for flux at the midplane, so the particles diffusing through the separatrix are effectively ignored.

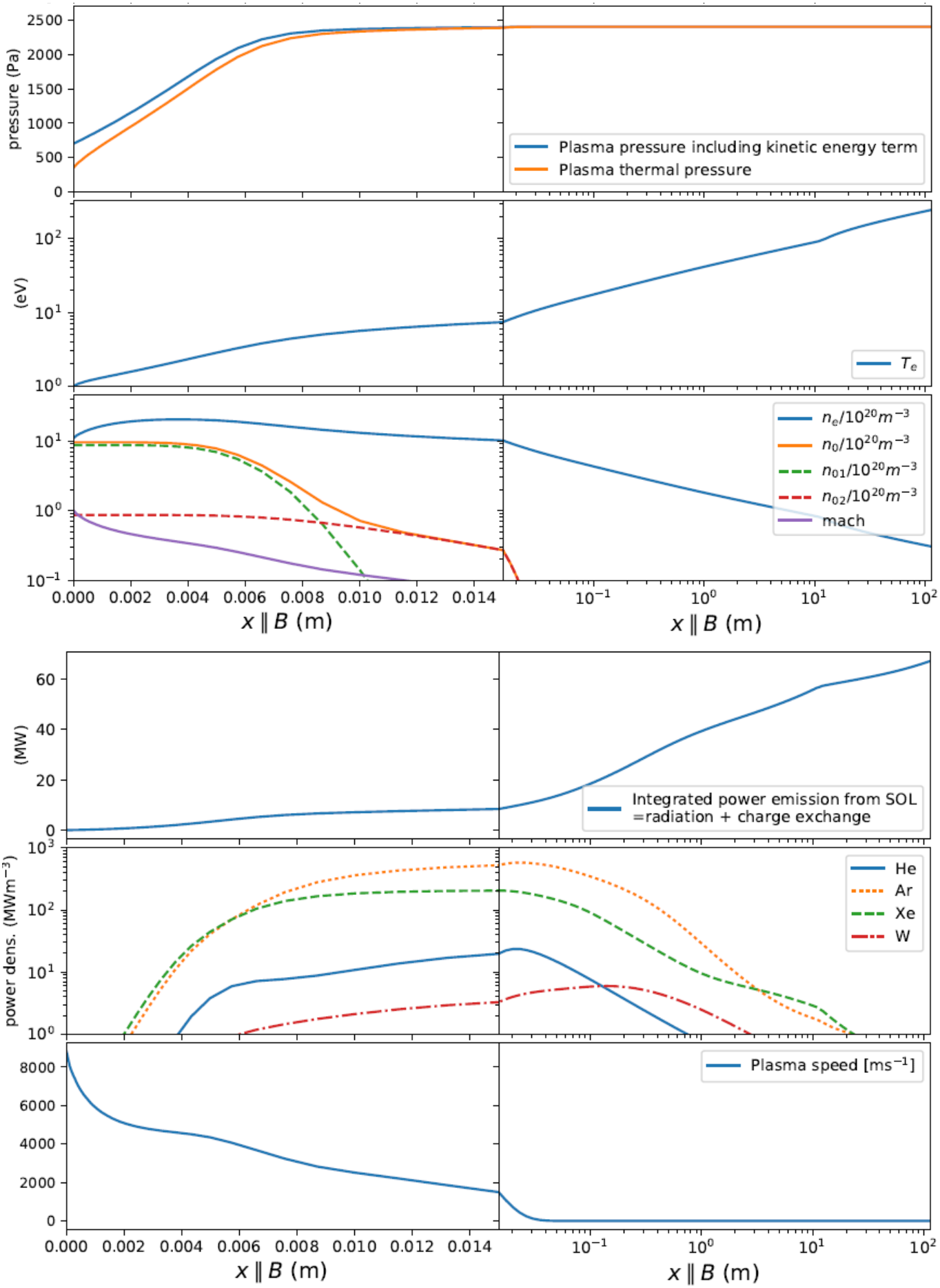

Figure 4. Parameters in the SOL. x = distance from the divertor target, measured along the field line. The left-hand graphs show the region near the target, and the right-hand graphs show the remainder of the flux tube up to the midplane. 'mach' = Mach number, 'He' = power density of radiation from helium, etc. Impurity concentrations in main plasma (ion density / electron density): He = 7.10×10^{-2}, Ar = 1.51×10^{-3}, Xe = 3.07×10^{-4}, W = 5×10^{-5}. SOL enrichment: He = 0.4, other impurities = 5.

Figure 5 shows the results from a PROCESS solution as the target temperature is reduced from 20 to 2 eV. From 12 to 2 eV the optimiser has achieved this by increasing the argon concentration and the major radius very slightly. The net electric power is fixed, effectively fixing the fusion power. Increasing the major radius increases the area of the divertor target, and also has a small effect on confinement, with a knock-on effect on the power conducted through the separatrix. These modest upstream changes are sufficient to reduce the target power density from 6.0 to 3.3 MW/m^2, although the contribution due to isotropic losses from the adjacent part of the SOL (section 4) increases and becomes dominant below 5 eV. The minimum in the argon curve suggests that two different solutions are possible for the same argon fraction in this strongly non-linear regime – more details in section 7. Divertor impurity concentrations are higher by the enrichment factors in Table 4.

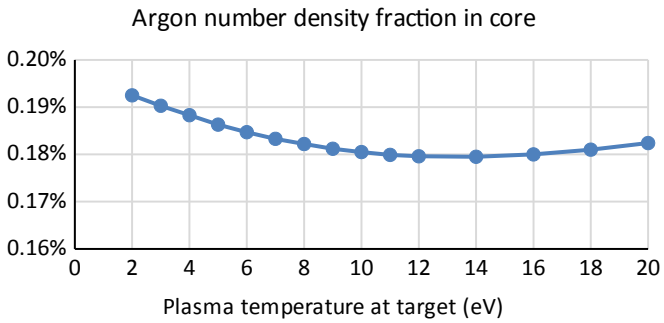

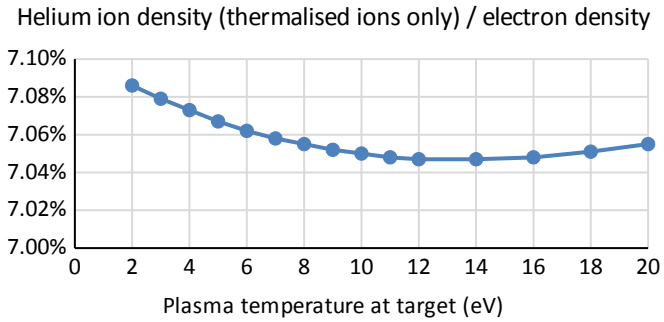

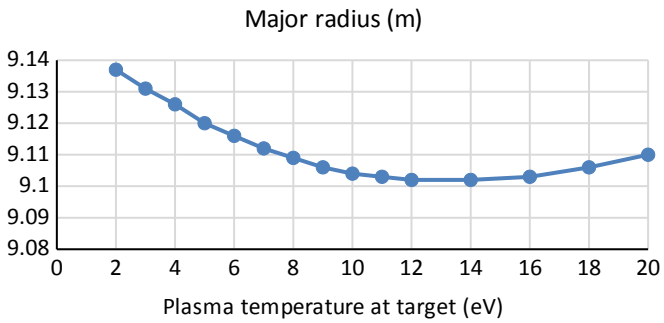

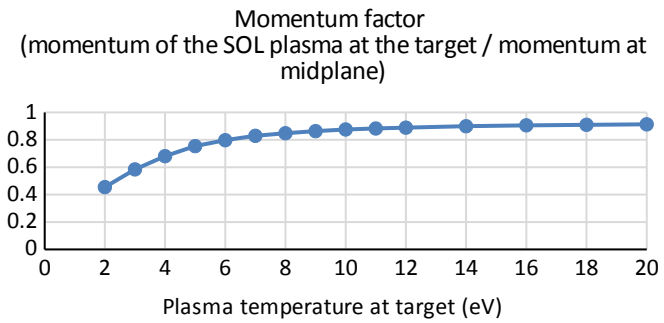

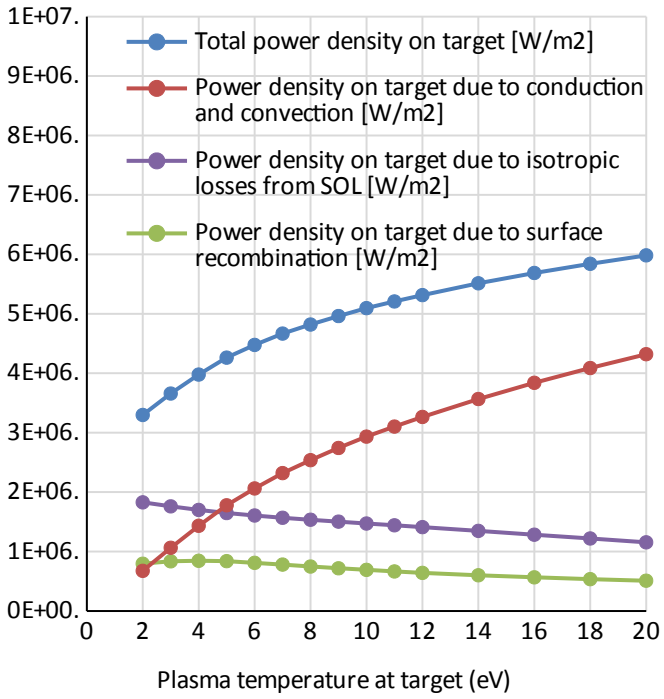

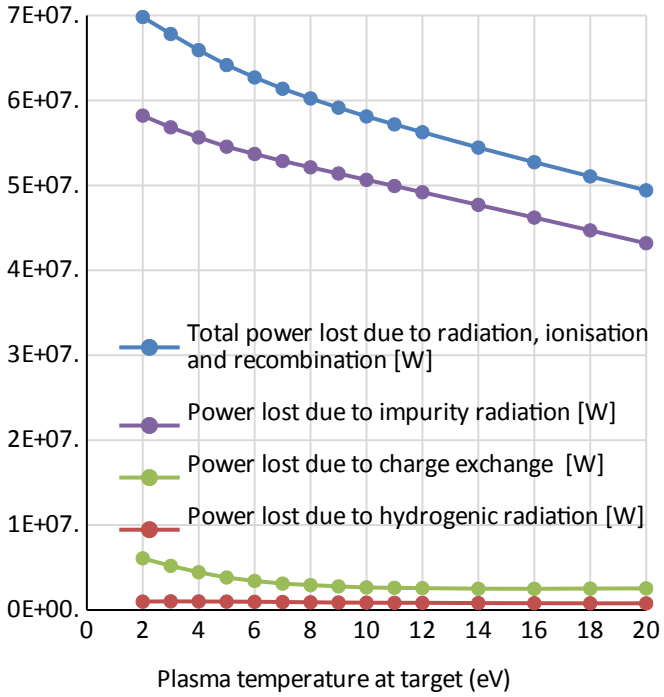

Figure 5. Parameters for confined plasma and divertor target as the temperature at the target varies from 20 to 2 eV.

If the enrichment factor is reduced, the optimiser compensates by increasing both the helium and the seeded impurity concentrations in the core, leading to greater fuel dilution. The mean plasma density also falls. Both of these effects reduce the fusion power per unit volume, leading to an increase in major radius, as shown in Figure 6.

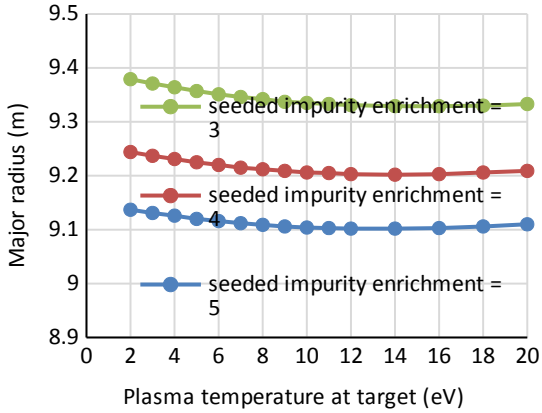

Figure 6. Plasma major radius for different values of the enrichment of Ar, Xe and W in the divertor relative to the confined plasma. Helium enrichment in SOL = 0.4.

Table 5. Selected PROCESS inputs and bounds

Figure of Merit	Plasma major radius
Burn time	= 7186 s
Net electric power	500 MW
Injected power (heating and current drive)	≤ 50 MW
He concentration	≥ 0.01
W concentration	5×10^{-5}–
Xe concentration	2.58×10^{-4}–
Argon concentration	≥ 10^{-4}–

7. Approach to detachment

The model describes the behaviour of a simplified SOL as it approaches detachment. The atomic data has not been supplied below 1 eV, so it is not possible to explore complete detachment, where the temperature at the target would be << 1 eV. Figure 7 shows the trends as the argon concentration is increased. A discontinuous transition is observed between an attached state with very little loss of momentum, and a state where 70% of the momentum is lost and the plasma temperature at the target hits the lower bound of the simulation (1.1 eV in this case). We suggest that this latter state has properties similar to the true detached state. Above a critical argon fraction multiple solutions exist. The two branches represent a SOL with high temperature and thermal conductivity and low temperature gradient, and one with low temperature and thermal conductivity causing a high temperature gradient. The individual solution branches can be explored by setting appropriate bounds for the adjustable parameters. Otherwise the solutions jump from one branch to another, causing the discontinuity shown. PROCESS solutions specifying that the target temperature is less than 20 eV will use the low temperature branch, as in Figure 5. (Although the PROCESS solver was used, the plasma geometry and most of the main plasma parameters were fixed, and the optimiser was effectively disabled.)

A discontinuous transition of this type is not usually observed in experimental scans, because adding more impurities typically leads to a decrease in the midplane separatrix density. In these simulations, in contrast, the separatrix density is held constant at 50% of the Greenwald density.

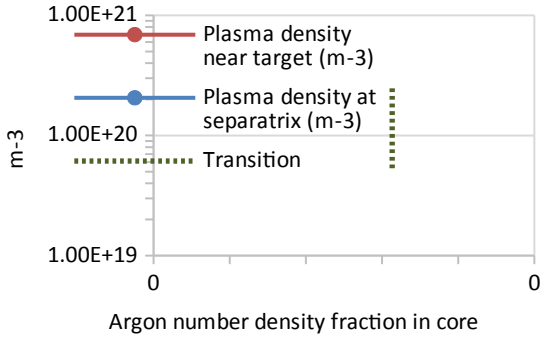

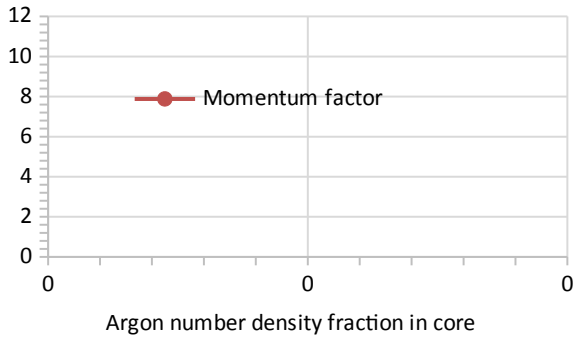

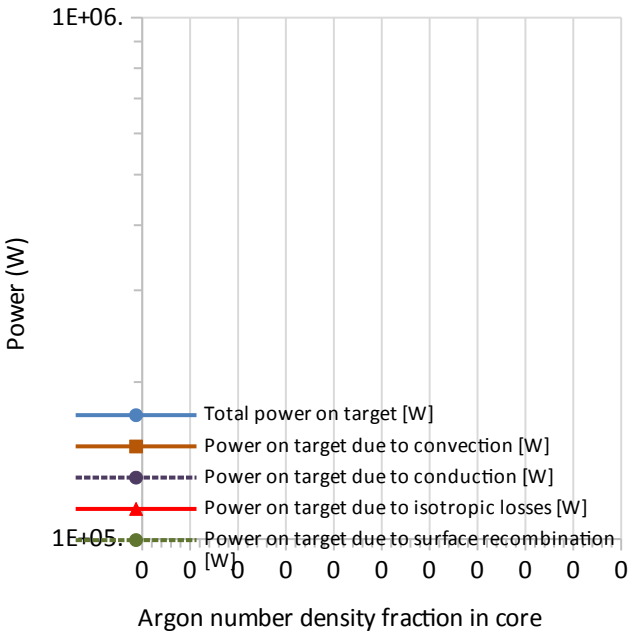

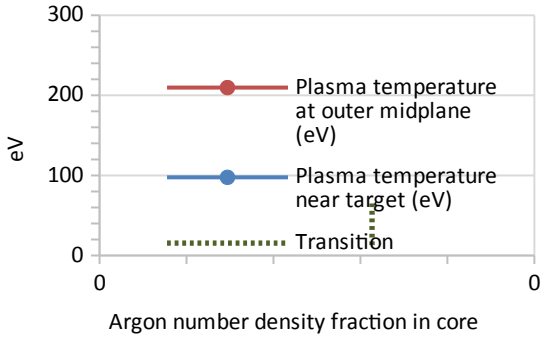

Figure 7. Parameters of the SOL and main plasma for varying argon fraction in (argon ions/electrons). Above a critical argon fraction multiple solutions exist. The discontinuous transition shown in the plot of power on target is represented by the dotted green line in the first and last plots. No solutions were found for argon fraction > 0.0020. The plasma temperature at the target was limited by the lower bound 1.1 eV. The optimiser was effectively disabled. Major radius 9.38 m, electron density (volume average) 7.165×10^{19} m^{-3}, electron temperature (volume average) 12.76 keV, vacuum toroidal field at plasma axis 4.916 T, Xe concentration = 2×10^{-4}, W concentration = 5×10^{-5}.

8. Conclusions

Integrating a fast one-dimensional scrape-off layer model into a systems code allows optimised reactor scenarios to be obtained while taking divertor conditions into account, at the cost of increasing the time required to obtain an optimised design from a few seconds to about one minute. An integrated core/divertor solution was found with a core Ar concentration below 0.2 % and a divertor Ar enrichment of a factor 5. The W concentration is set to 5×10^{-5}, and the Xe concentration is 2.6×10^{-4}. Systems studies frequently find that the optimised reactor design is very insensitive to the individual parameters [14]. This is the case in the example given in section 6, where an increase in major radius of 27 mm and other tiny changes are sufficient to reduce the target power density from 6.0 to 3.3 MW/m^2, and the target temperature from 20 to 2 eV. Nevertheless a physically reasonable SOL model makes the design more credible, and imposes more realistic limits on the impurity fractions.

The isotropic emission of fast neutrals due to charge exchange from the part of the SOL adjacent to the target dominates the total power density on the target when the plasma temperature is reduced below 5 eV.

The model appears to describe the behaviour of the SOL as it approaches detachment. More careful consideration of the physics at temperatures below 1 eV would be required to describe detached conditions.

9. Acknowledgments

We would like to thank Martin O'Mullane and R. Wenninger. This work has been carried out within the framework of the EUROfusion Consortium and has received funding from the Euratom research and training programme 2014-2018 under grant agreement No 633053 and from the RCUK Energy Programme [grant number EP/P012450/1]. To obtain further information on the data and models underlying this paper please contact PublicationsManager@ccfe.ac.uk. The views and opinions expressed herein do not necessarily reflect those of the European Commission.

10. Appendix: Supplementary data

The output file, including the input data, for the PROCESS runs used are available in Supplementary Data.

11. References

1. Kallenbach A, Bernert M, Dux R, Reimold F, Wischmeier M. Analytical calculations for impurity seeded partially detached divertor conditions. Plasma Phys Control Fusion. 2016;58(4):045013. http://iopscience.iop.org/article/10.1088/0741-3335/58/4/045013
2. Kovari M, Kemp R, Lux H, Knight P, Morris J, Ward DJ. "PROCESS": A systems code for fusion power plants—Part 1: Physics. Fusion Eng Des. 2014 Dec;89(12):3054–69. http://www.sciencedirect.com/science/article/pii/S0920379614005961
3. Loarte a, Lipschultz B, Kukushkin a. ., Matthews G., Stangeby P., Asakura N, et al. Chapter 4: Power and particle control. Nucl Fusion. 2007 Jun 1;47(6):S203–63. http://stacks.iop.org/0029-5515/47/i=6/a=S04?key=crossref.171e8579115c86813cca00821182da6b
4. Wischmeier M, Groth M, Kallenbach A, Chankin AV, Coster DP, Dux R, et al. Current understanding of divertor detachment: Experiments and modelling. J Nucl Mater. 2009 Jun 15;390-391:250–4. https://www.sciencedirect.com/science/article/pii/S002231150900107X
5. Subba F, Aho-Mantila L, Coster D, Maddaluno G, Nallo GF, Sieglin B, et al. Modelling of mitigation of the power divertor loading for the EU DEMO through Ar injection. Plasma Phys Control Fusion. 2018 Mar 1;60(3):035013. http://stacks.iop.org/0741-3335/60/i=3/a=035013?key=crossref.87900193069278ae7d690b41ee6eebbd
6. Asakura N, Hoshino K, Suzuki S, Tokunaga S, Someya Y, Utoh H, et al. Studies of power exhaust and divertor design for a 1.5 GW-level fusion power DEMO. Nucl Fusion. 2017 Dec 1;57(12):126050. http://stacks.iop.org/0029-5515/57/i=12/a=126050?key=crossref.d5b9ab574f3af76f70e12260f11c19ca
7. Massey HSW, Burhop EHS. Electronic And Ionic Impact Phenomena, page 252 of pdf file. Oxford University Press; 1951. https://archive.org/details/electronicandion031580mbp
8. Huber A, Chankin A V. Scaling for the SOL/separatrix $\chi_\perp$ following from the heuristic drift model for the power scrape-off layer width. Plasma Phys Control Fusion. 2017;59(6):064007. http://stacks.iop.org/0741-3335/59/i=6/a=064007?key=crossref.d5e1d23ed5541dd300b62d4aefb0480b
9. Dux R, Loarte A, Fable E, Kukushkin A. Transport of tungsten in the H-mode edge transport barrier of ITER. Plasma Phys Control Fusion. 2014 Dec 1;56(12):124003. http://stacks.iop.org/0741-3335/56/i=12/a=124003?key=crossref.397bb02568e4450034b62adb612703ab
10. Shampine LF, Gordon MK (Marilyn K. Computer solution of ordinary differential equations : the initial value problem. W.H. Freeman; 1975. 318 p. https://people.sc.fsu.edu/~jburkardt/f_src/ode/ode.html
11. Stangeby PC. The plasma boundary of magnetic fusion devices. Institute of Physics Pub; 2000. 717 p.

12. Zhongshi Yang, Qian Xu, Rongjie Hong, Qiang Li, Guang-Nan Luo. Molecular dynamics simulation of low-energy atomic hydrogen on tungsten surface. Fusion Eng Des. 2010 Dec 1;85(7-9):1517–20. http://www.sciencedirect.com/science/article/pii/S0920379610001596?via%3Dihub
13. Kallenbach A. Overview of ASDEX Upgrade results. Nucl Fusion. 2017;57(10):102015. http://stacks.iop.org/0029-5515/57/i=10/a=102015?key=crossref.b51cc0eec82d6fb09a50d1e7dccee4e2
14. Kovari M, Fox F, Harrington C, Kembleton R, Knight P, Lux H, et al. “PROCESS”: A systems code for fusion power plants – Part 2: Engineering. Fusion Eng Des. 2016 Mar;104:9–20. http://www.sciencedirect.com/science/article/pii/S0920379616300072